LIFELINE
EMERGENCY and SAFETY
Research Article

Resistivity-enhanced multi-physics machine learning framework for dynamic stress prediction in high sensitive UHPC

Bin Liao[1], Lin Chi[1,✉], Chenlong Qiang[1], Rui Zhu[1], Shicheng Cui[1], Lifei Zhang[2]

Cite this article: Liao B, Chi L, Qiang C L, et al. *Lifeline Emergency and Safety* 2026, **1**: 9660012. https://doi.org/10.26599/LLES.2025.9660012

ABSTRACT: Machine learning provides powerful capabilities for modeling complex nonlinear relationships in cement-based materials, particularly in predicting mechanical behavior. Traditional compressive stress prediction models for UHPC rely predominantly on strain or displacement inputs and suffer from limited accuracy. Critically, electrical resistivity, as an intrinsic material property, demonstrates strong correlations with stress-induced microstructural evolution. This study proposes a machine learning framework for dynamic compressive stress prediction in high sensitivity ultra-high performance concrete (HS-UHPC) integrated with carbon nanotubes. Three distinct machine learning algorithms, double-layer neural network (DLNN), boosting tree (BT), and squared exponential Gaussian process regression (SE-GPR) were employed to establish compressive stress prediction model of HS-UHPC. Results demonstrated that incorporating resistivity measurements alongside displacement data significantly enhanced predictive accuracy, increasing R^2 by 0.06 compared to displacement-only models. The SE-GPR model achieved the highest performance (R^2 = 0.85, RMSE = 0.11) under dual-input conditions, exhibiting a 41.1% reduction in mean absolute error compared to displacement-only models. Integrating resistivity as a key input parameter fundamentally enhances model performance by directly capturing stress-driven microstructural changes, establishing a superior sensing paradigm for ML-based structural health monitoring.

KEYWORDS: Machine learning; ultra-high performance concrete (UHPC); resistivity; compressive stress

1 Introduction

Ultra-high performance concrete (UHPC) has gained prominence in structural engineering due to its exceptional compressive strength, superior durability, and remarkable impermeability[1,2], finding extensive applications in long-span bridges and super-tall buildings[3-6]. However, stress concentration phenomena under prolonged dynamic loading and corrosive environments pose catastrophic failure risks in these complex structures, necessitating real-time compressive stress monitoring for accurate lifespan assessment. However, traditional piezoelectric or fiber-optic sensors struggle to meet the requirements for long-term stable monitoring due to insufficient durability, high cost, and incompatibility with concrete matrix deformation[7-9]. Achieving passive operation and high-precision stress prediction through material intrinsic properties has emerged as a critical challenge in the structural health monitoring field.

Recent advances in machine learning (ML) have demonstrated potential for deciphering the nonlinear constitutive relationships of UHPC. Mohammad et al.[10] established an Extra trees-based stress model (R^2 = 0.80), while Pishro et al.[11] achieved 60% accuracy using linear regression. Nguyen et al.[12] incorporated mix design and mixing duration to predict interfacial yield stress ($R^2 \approx$ 0.83). However, current UHPC stress prediction models exhibit limited accuracy, primarily due to reliance on mixture proportions and deformation parameters as inputs. Although Hiew et al.[13] used strain measurements for stress prediction, extensive data samples were still required. Similarly, neural networks by Jiang et al.[14] achieved enhanced accuracy (R^2 = 0.89) but exhibited similar constraints. This limitation stems from insufficient correlation between inputs and material damage evolution, motivating exploration of intrinsic parameters characterizing microstructural evolution dynamics.

A strong correlation between variations in concrete electrical resistivity and internal stress distribution has been demonstrated. Experimental evidence indicated a 15.65% reduction in resistivity when compressive stress increases from 20 MPa to 100 MPa[15,16]. This finding suggests resistivity, as an intrinsic material parameter, may provide highly informative features for machine learning models by reflecting microstructural damage evolution. Consequently, resistivity-based static intensity prediction prediction has been explored. Feng et al.[17] developed a CPO-XGBoost model incorporating resistivity measurements to predict compressive strength of cementitious materials, achieving superior accuracy (R^2 = 0.957, RMSE = 0.312 MPa, MAE = 0.251 MPa). Similarly, Chi et al.[18] observed a 0.01 R^2 improvement using resistivity-modified prediction models. However, the potential for structural dynamic monitoring was revealed by the development of smart concrete systems. Chen et al.[19] designed smart sensing

[1] School of Environment and Architecture, University of Shanghai for Science and Technology, Shanghai 200093, China. [2] School of Environment and Civil Engineering, Dongguan University of Technology, Dongguan 523808, China.

✉ Corresponding author. E-mail: chilin@usst.edu.cn

Received: June 11, 2025; Revised: July 30, 2025; Accepted: August 29, 2025

concrete with piezoelectric and carbon fibers, achieving a minimum detectable strain of 16.9 με. Viet et al.[20] monitored the crack damage in smart UHPC through dynamic electrical resistivity measurement, which confirms a real-time correlation between dynamic resistivity variation and the stress-induced damage progression. Although electrical resistivity has been demonstrated as an effective dynamic damage indicator, a framework for predicting stress via real-time resistivity variation remains unestablished.

This study proposed a multi-physics coupled stress prediction model based on high sensitive UHPC (HS-UHPC). Mechanical and electrical physical domains were concurrently integrated within the multi-physics framework. Macroscopic deformation characteristics under compressive loading were quantified through in-situ displacement monitoring. Simultaneously, stress-induced microstructural alterations were captured via resistivity variations. Through systematic integration of mix proportion parameters, displacement characteristics, and resistivity features combined with machine learning algorithms, we established a dynamic stress prediction framework. Sensitivity analysis quantitatively evaluates the coupling weights among multi-physical fields. The proposed methodology not only improves prediction accuracy for dynamic stresses compared to conventional strain-based models, but also provides theoretical foundations for intelligent design and engineering applications of self-sensing UHPC.

2 Dataset

This study developed a compressive stress prediction model utilizing 446 experimental datasets from HS-UHPC under uniaxial loading. The input parameters, as detailed in Table 1, consist of material mix proportions and mechanical response indicators, with UHPC compressive stress serving as the output. Specifically, resistivity and displacement were acquired through real-time mechanical response monitoring; steel fiber and carbon nanotube (CNT) inputs corresponded to actual mix proportions. To evaluate the contribution of electrical parameters, two input configurations were implemented. Dataset I contains mix proportions and displacement. Dataset II contains mix proportions, displacement and resistivity.

Table 1 Input parameters.

	Count	Max	Min
Resistivity	446	30,145	21,150
Displacement		7.81	0
Steel fiber		1.6	1.2
CNT		0.2	0

This study employed three machine learning algorithms, double-layer neural network (DLNN), boosting tree (BT), and squared exponential gaussian process regression (SE-GPR), to develop the compressive stress prediction models of UHPC. Dimensional inconsistencies were addressed through normalization prior to model development, with subsequent denormalization restoring physical interpretability to the outputs. Model performance was evaluated using dual metrics: root mean square error (RMSE, Eq. (1)) measuring absolute deviations between predicted and experimental values, and coefficient of determination (R^2, Eq. (2)) assessing linear correlation strength. To ensure robust generalization capability, a rigorous 10-fold cross-validation protocol was implemented. The dataset was randomly partitioned into 10 mutually exclusive subsets, with 9 subsets used for training and the remaining subset for validation in each iteration. This cyclic process continued until all subsets had served as validation data.

$$\mathrm{RMSE}=\sqrt{\sum\nolimits_{i=1}^{n}(e_i-p_i)^2/n} \tag{1}$$

$$R^2=\left[\frac{\sum\nolimits_{i=1}^{n}(e_i-\overline{e_i})(p_i-\overline{p_i})}{\sqrt{\sum\nolimits_{i=1}^{n}(e_i-\overline{e_i})^2\sum\nolimits_{i=1}^{n}(p_i-\overline{p_i})^2}}\right]^2 \tag{2}$$

where n represents the total number of samples; e_i and p_i are experimental and predicted values, respectively; $\overline{e_i}$ and $\overline{p_i}$ are averages of e_i and p_i, respectively.

3 Machine learning models

3.1 Double-layer neural network

The double-layer neural network (DLNN), foundational to deep learning, enables low-dimensional representation of high-dimensional data and non-linear function approximation[21,22]. Structurally, it comprises an input layer, a single hidden layer, and an output layer, formulated as

$$f(x;\theta)=W_2\sigma(W_1x+b_1)+b_2 \tag{3}$$

where, W_1 and W_2 represent weight matrices, b_1 and b_2 are bias terms, and σ is a non-linear activation function.

The hidden layer neuron count was optimized through Bayesian hyperparameter search across 50 iterations, with units ranging from 8 to 32. A nonlinear rectified linear unit activation function was systematically selected through validation root mean square error minimization during ten-fold cross-validation. Adaptive moment estimation was applied for training, featuring an initial learning rate of 0.001 decayed by a factor of 0.2 every 100 epochs. Concurrently, L_2 regularization strength was tuned within the 10^{-4} to 10^{-2} range for overfitting prevention.

3.2 Boosting tree (BT)

The boosting tree algorithm, an efficient ensemble learning framework, approximates complex functions through iterative optimization of additive models[23,24]. Prediction residuals from prior models are progressively corrected using gradient descent, yielding a combined model with strong generalization capability. Convergence of the algorithm is determined by the weak-learning hypothesis of base learners and convexity of the loss function. Owing to its non-parametric nature, high-order interaction effects and nonlinear patterns are adaptively captured while model interpretability is maintained. In this study, sequential learners with adaptive learning rate decay were employed in BT model. Minimum leaf size was optimized between 4–20 observations, enforcing early stopping after 20 unchanged iterations.

3.3 Squared exponential gaussian process regression (SE-GPR)

The squared exponential gaussian process regression (SE-GPR), being a non-parametric Bayesian model, realizes the probabilistic modeling of the continuous function space and uncertainty quantification through the covariance structure driven by the kernel function[25,26]. Based on the gaussian process framework, it assumes that the target function follows a Gaussian prior distribution with a mean of zero and a covariance defined by the squared-exponential kernel. Its mathematical form is expressed as

$$k(x_i, x_j) = \sigma_{\mathrm{f}}^2 \exp\left(-\frac{1}{2l^2}||x_i - x_j||^2\right) + \sigma_{\mathrm{n}}^2\sigma_{ij} \tag{4}$$

where, σ_{f}^2 represents the signal variance, l is the length scale, σ_{n}^2 is the noise variance, and δ_{ij} is the Kronecker delta function.

In this study, an isotropic squared exponential kernel was applied in the Gaussian process regression. Kernel hyperparameters (signal variance, noise variance, length scale) were optimized through exact log-likelihood maximization using quasi-Newton optimization.

4 Machine learning prediction

4.1 Parameter input

Enhanced compressive stress prediction is enabled by the parameter diversity illustrated in Figures 1(a)–1(d). Compressive stress values are predominantly distributed within the 10–90 MPa range (constituting 80% of samples), allowing common condition patterns to be effectively learned. Exclusion of extreme cases during prediction is prevented by the inclusion of limited high- and low-stress data. Resistivity values are clustered bimodally (0–70 Ω·m and 100–150 Ω·m), corresponding to ordinary and carbon nanotube (CNT)-incorporated composites respectively, enabling material differentiation to be achieved. Displacement data are uniformly distributed across 0–1.5 mm, eliminating concentration bias and ensuring comprehensive pressure-change relationships are captured. CNT content is discretely assigned (0%, 0.1%, 0.15%, 0.2%), facilitating optimal reinforcement ratios to be identified and comparative CNT-stress relationships to be analyzed. Collectively, these distributions ensure robust pattern recognition across frequent scenarios while generalization capability for complex conditions is maintained, yielding reliable predictions.

4.2 Sensitivity analysis

Analysis of the correlation heat map reveals distinct relationships between input parameters and compressive stress, as shown in Figure 2. Notably, displacement exhibited the strongest correlation (coefficient=0.51), confirming its critical role in compressive stress prediction. Resistivity demonstrated a moderate positive correlation (coefficient=0.20), suggesting its value as a predictive indicator. Crucially, the low correlation coefficient between resistivity and displacement (0.09) indicated high mutual independence, enabling their use as complementary variables to enhance model accuracy. Consequently, resistivity and displacement served as core input parameters that both independently explained compressive stress variation and mitigate overfitting risks through low collinearity. Additionally, despite weak direct correlations between steel fiber and CNT content and compressive stress, both parameters were retained in the model due to their established roles in electromechanical mediation pathways. Specifically, steel fiber content was moderately positively correlated with resistivity (coefficient = 0.30), whereas CNT concentration exhibited a strong inverse correlation (coefficient = −0.66). Given the significant correlation between resistivity and compressive stress (coefficient = 0.20), steel fiber and CNT content were recognized as critical upstream variables governing the electrical response. Their influence was exerted indirectly through resistivity modulation. Conduction pathways

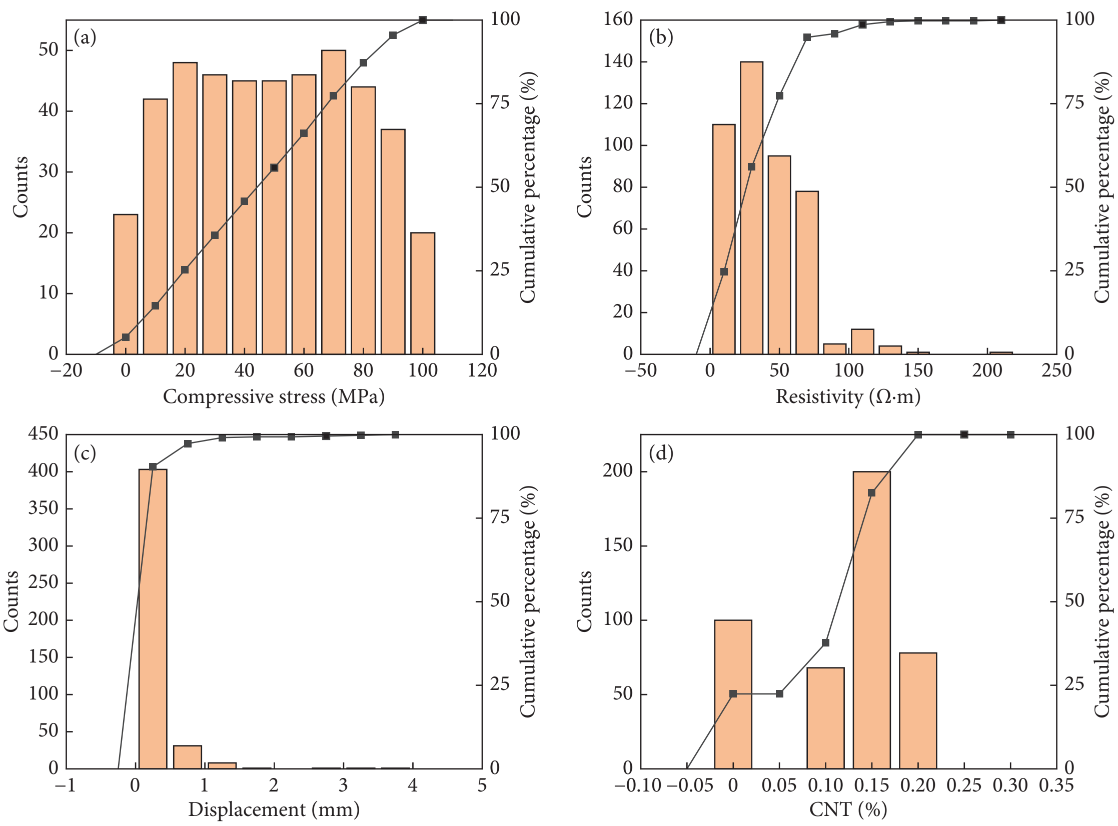

Fig. 1 Statistical parameters of data distribution: (a) Compressive stress; (b) resistivity; (c) displacement; (d) CNT content.

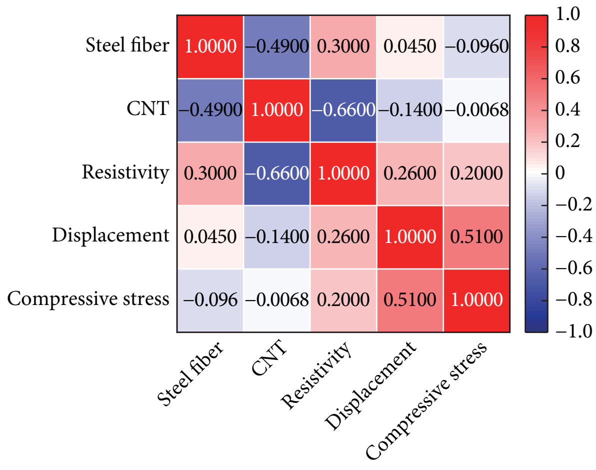

Fig. 2 Sensitivity analysis.

were modified by steel fiber primarily via crack-bridging effects, while percolation networks established by CNTs were distorted under load, thereby mediating the resistivity-stress coupling[27]. Therefore, data acquisition and parameter calibration for compressive stress prediction models should prioritize these parameters.

4.3 Prediction results

Figure 3 presents the compressive stress prediction performance of three computational models (DLNN, BT, and SE-GPR) for HS-UHPC under compression, comparing displacement inputs versus combined displacement and resistivity inputs. Under dual-input scenarios incorporating resistivity and displacement parameters, enhanced agreement between predicted and experimental values was demonstrated across all models compared to single-parameter conditions, with significantly reduced data points exceeding the ±10% error threshold. Notably, the SE-GPR model exhibited tighter prediction clustering

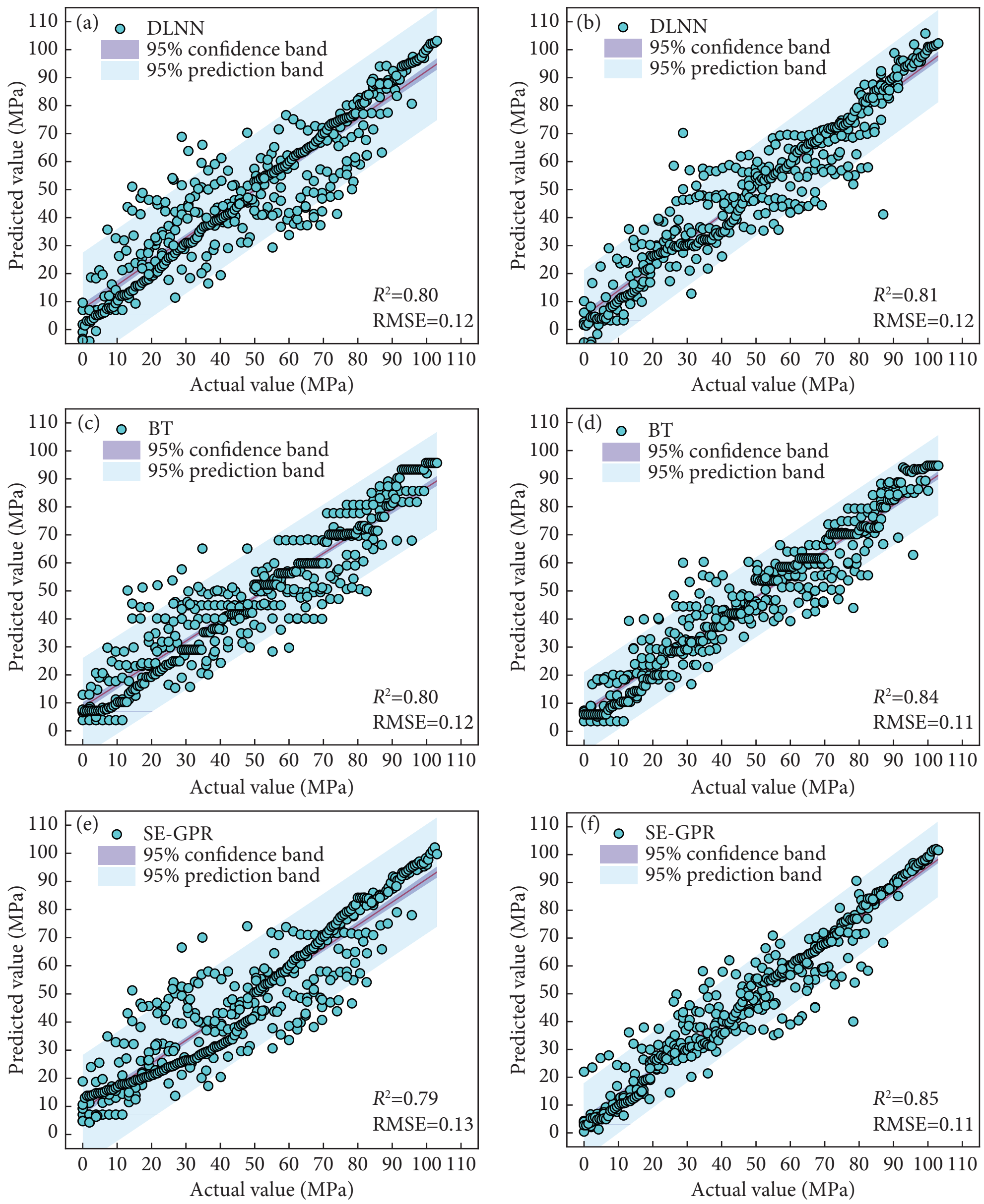

Fig. 3 Prediction results of compressive stress: (a), (c), (e): predicted by database I; (b), (d), (f): predicted by database II.

(Figure 3(f)), where metric improvements from $R^2 = 0.79$ to 0.85 and RMSE reduction from 0.13 to 0.11 were achieved. These results confirm that electro-mechanical coupling behavior during compressive loading is effectively captured through resistivity integration. This finding substantiates the necessity of multi-physics collaborative modeling, particularly for electrically sensitive materials where resistivity variations may indirectly reflect internal microcrack propagation and stress redistribution processes.

Substantial variation in model sensitivity to input parameters was observed. While R^2 improvements for neural network and boosted tree models under dual inputs were modest (0.01 and 0.04, respectively), greater enhancement was exhibited by SE-GPR. Analysis of data distributions revealed distinct behaviors. Stronger dependency on dual-input parameters was demonstrated by DLNN (Figure 3(b)), evidenced by localized deviations from experimental data under single-input conditions that were substantially mitigated through dual-parameter integration—a phenomenon potentially attributable to superior high-dimensional feature fusion capability. In contrast, inherent stability was exhibited by the BT model even with single-input configurations (Figure 3(c)), with further error reduction achieved upon resistivity incorporation (Figure 3(d)). This suggested that nonlinear relationship characterization is effectively optimized through hierarchical feature interactions within its tree architecture.

In conclusion, it is demonstrated that synergistic combination of resistivity and displacement inputs is essential for enhancing compressive stress prediction accuracy in electrically sensitive UHPC. Optimal comprehensive performance under dual-parameter conditions is achieved by the SE-GPR model, reflecting the superior capability of Gaussian process regression in modeling multivariate nonlinear relationships. These results confirm the significance of multiphysics parameter coupling in smart material systems.

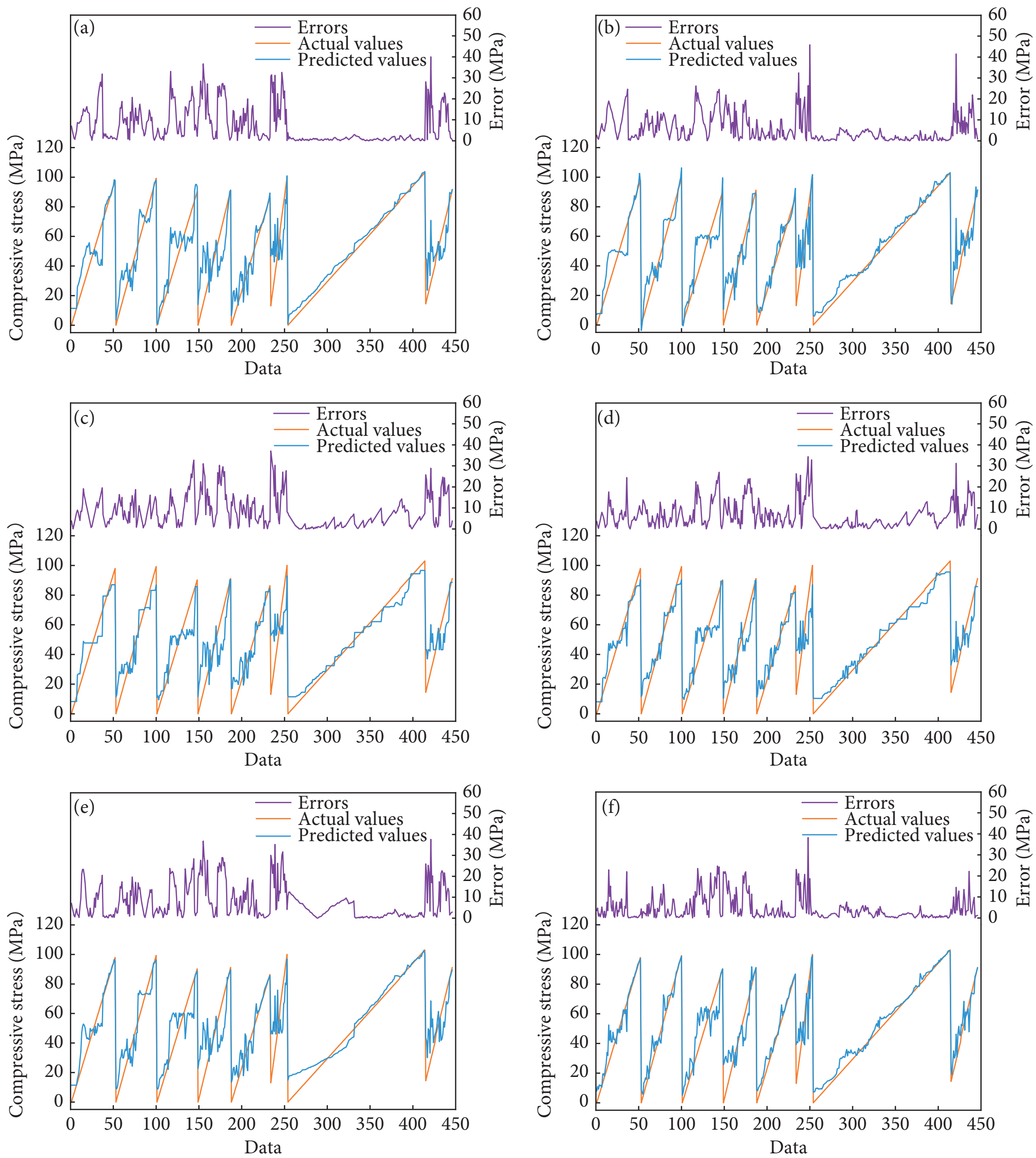

Fig. 4 Actual value, predicted value and errors of models: (a), (c), (e): predicted by database I; (b), (d), (f): predicted by database II.

4.4 Error analysis

Figure 4 compares the compressive stress prediction errors of deep neural network (DLNN), gradient boosted tree (BT), and squared exponential Gaussian process regression (SE-GPR) of HS-UHPC, evaluated across displacement-only and displacement-resistivity dual-input scenarios. The SE-GPR model achieved optimal comprehensive performance under dual-input conditions, exhibiting a 41.1% reduction in mean absolute error (MAE) compared to single-input scenarios, along with the narrowest error distribution. This superiority stems from its Bayesian nonparametric framework utilizing a squared exponential kernel, which adaptively quantifies uncertainty through covariance matrix regularization, effectively mitigating overfitting in complex nonlinear relationships. The BT model reduced MAE by 12.3% via iterative feature interaction optimization, though residual deviations persisted in high-stress regions (>120 MPa), presumably attributable to insufficient coverage of extreme microcrack propagation patterns in training data. While the DLNN model attained a 16.9% error reduction, its performance was constrained by nonconvex optimization challenges in high-dimensional latent space, leading to sensitivity to initial parameters and occasional anomalous predictions. Common error sources include resistivity measurement noise (particularly in high-frequency bands) and dielectric response discretization induced by fiber orientation heterogeneity. These findings collectively demonstrate superior accuracy of SE-GPR and robustness among the three modeling approaches.

5 Conclusions

(1) Incorporation of resistivity as an additional input parameter enhanced the predictive accuracy of SE-GPR for compressive stress of HS-UHPC, yielding a 0.06 improvement in R^2. This confirms that resistivity serves as a critical electrical feature to complement stress sensing in UHPC, providing a theoretical foundation for intelligent monitoring and design of self-sensing concrete systems.

(2) Significant prediction error reduction was achieved across all models through synergistic use of resistivity and displacement inputs. Under dual-parameter conditions, the SE-GPR model exhibited a 41.1% reduction in mean absolute error (MAE) compared to displacement-only input; corresponding reductions of 12.3% and 16.9% were observed for BT and DLNN models, respectively.

(3) Among the evaluated algorithms, the highest predictive accuracy for compressive stress of HS-UHPC was demonstrated by the SE-GPR model, achieving an R^2 value of 0.85.

Acknowledgement

This work was supported by Guangdong Provincial Key Laboratory of Intelligent Disaster Prevention and Emergency Technologies for Urban Lifeline Engineering (2022) under Grant No. 2022B1212010016.

Author contribution statement

Bin Liao is responsible for Writing original draft, Methodology, Data curation; Lin Chi is responsible for Supervison, Funding acquisition, Methodology; Chenlong Qiang is responsible for Writing-review and editing, Conceptualization; Rui Zhu is responsible for Writing-review and editing, Investigation; Shicheng Cui is responsible for Investigation, Experiment; Lifei Zhang is responsible for Supervison, Validation.

Data availability

The data that support the findings of this study is available from the corresponding author upon reasonable request.

Use of AI statement

None.

Declaration of competing interest

The author(s) have no competing interests to declare that are relevant to the content of this article.

References

[1] Yoo, D. Y., Banthia, N., Yoon, Y. S. (2024). Recent development of innovative steel fibers for ultra-high-performance concrete (UHPC): a critical review. *Cement and Concrete Composites*, 145: 105359.

[2] Tu, L., Zhao, H., Tan, C. J., Hu, J. D., Cao, J. Q., Wu, S. W. (2025). Tensile behavior of reinforced UHPC: effects of autogenous shrinkage and model of tensile capacity via deep learning-based symbolic regression. *Cement and Concrete Composites*, 160: 106019.

[3] Ghahsareh, F. M., Zhang, Q. H., Poorghasem, S., Shah, H. A., Guo, P. W., Christodoulatos, C., Meng, W. N., Bao, Y. (2025). Cradle-to-grave life-cycle assessment of ultra-high-performance concrete (UHPC) beams based on real-time monitoring data. *Journal of Cleaner Production*, 495: 145098.

[4] Richard, P., Cheyrezy, M. (1995). Composition of reactive powder concretes. *Cement and Concrete Research*, 25(7): 1501–1511.

[5] Jiang, K. D., Wang, X., Ding, L. N., Chen, Z. Y., Huang, H., Liu, X., Liu, J. X., Wu, Z. S. (2023). Mechanical properties of multi-scale mono/hybrid non-metallic fiber-reinforced ultra-high performance seawater sea-sand concrete. *Construction and Building Materials*, 401: 132922.

[6] Zhou, M., Wu, Z. M., Ouyang, X., Hu, X., Shi, C. J. (2021). Mixture design methods for ultra-high-performance concrete—a review. *Cement and Concrete Composites*, 124: 104242.

[7] Tan, X., Du, J., Zhang, Q. H., Meng, W. N., Bao, Y. (2024). Monitoring restrained shrinkage and cracks of ultra-high-performance concrete (UHPC) using distributed fiber optic sensors. *Construction and Building Materials*, 422: 135789.

[8] Yazdizadeh, Z., Marzouk, H., Hadianfard, M. A. (2017). Monitoring of concrete shrinkage and creep using Fiber Bragg Grating sensors. *Construction and Building Materials*, 137: 505–512.

[9] Zhang, Y., Qin, Z. X., Luo, S. Z., Hyunjo, J., Zhang, S. Z. (2022). Design and application of partial immersion focused ultrasonic transducers for austenitic weld inspection. *Sensors*, 22(7): 2671.

[10] Barkhordari, M. S., Jaaz, H. A. G., Jawdhari, A. (2025). Data-driven machine learning forecasting and design models for the tensile stress-strain response of UHPC. *Structures*, 71: 107965.

[11] Amini Pishro, A., Zhang, S. Q., Hu, Q. X., Zhang, Z. R., Amini Pishro, M., Zhang, L. L., L'Hostis, A., Hejazi, F., Liu, Y. T., Zhao, Y. D. (2024). Advancing ultimate bond stress–slip model of UHPC structures through a novel hybrid machine learning approach. *Structures*, 62: 106162.

[12] Nguyen, T. D., Tran, T. H., Hoang, N. D. (2020). Prediction of interface yield stress and plastic viscosity of fresh concrete using a hybrid machine learning approach. *Advanced Engineering Informatics*, 44: 101057.

[13] Hiew, S. Y., Teoh, K. B., Raman, S. N., Kong, D., Hafezolghorani, M. (2023). Prediction of ultimate conditions and stress–strain

behaviour of steel-confined ultra-high-performance concrete using sequential deep feed-forward neural network modelling strategy. *Engineering Structures*, 277: 115447.

[14] Jiang, K. J., Han, Q., Bai, Y. L., Du, X. L. (2020). Data-driven ultimate conditions prediction and stress-strain model for FRP-confined concrete. *Composite Structures*, 242: 112094.

[15] Lee, S. Y., Le, H. V., Kim, D. J. (2019). Self-stress sensing smart concrete containing fine steel slag aggregates and steel fibers under high compressive stress. *Construction and Building Materials*, 220: 149–160.

[16] Wang, H., Wang, A., Wang, J., Zhang, J. Y., Du, T., Shen, J. L. (2025). Optimizing quaternary chemical additives and steel fiber dispersion in CSA cement based HPC for rapid repair engineering. *Construction and Building Materials*, 489: 142265.

[17] Feng, G. R., Zhan, M. N., Wang, Z. H., Qi, T. Y., Wang, Y., Mi, J. C. (2025). Prediction of layered UCS of cemented-gangue backfill material using hybrid intelligent models and electrical resistivity segregation monitoring method. *Materials Today Communications*, 46: 112631.

[18] Chi, L., Wang, M., Liu, K. H., Lu, S., Kan, L. L., Xia, X. M., Huang, C. D. (2023). Machine learning prediction of compressive strength of concrete with resistivity modification. *Materials Today Communications*, 36: 106470.

[19] Chen, X., Zhang, Z. L., Zhu, R. J., Huang, H. Y., Ran, Q. P., Wang, Z. M. (2025). Dynamic/static sensing based on piezoelectric/ piezoresistive smart sensing concrete. *Sensors and Actuators A: Physical*, 393: 116786.

[20] Viet Le, H., Pham, T. N., Dang, V. P., Dao, P. L., Nguyen, D. L., Tran, N. T., Kim, D. J. (2025). Damage sensing characteristics of smart ultra-high-performance concrete containing electrically conductive fiber and particle fillers under high compressive stress. *Sensors and Actuators A: Physical*, 383: 116242.

[21] Faiz, J., Haghdoust, V., Samimi, M. H. (2024). Physical, semi-physical and computational fluid dynamics thermal models of power transformers using artificial neural networks—A review. *International Communications in Heat and Mass Transfer*, 159: 108288.

[22] Patel, R., Li, W. Q., Smith, R. J., Clark, M. (2025). Developing neural networks to rapidly map crystallographic orientation using laser ultrasound measurements. *Scripta Materialia*, 256: 116415.

[23] Adamu, M., Sapkota, S. C., Das, S., Saha, P., Ibrahim, Y. E. (2025). An explainable boosting-based ensemble machine learning model for predicting the properties of date palm fiber reinforced concrete. *Sustainable Chemistry and Pharmacy*, 44: 101949.

[24] Ahmed, A. H. A., Jin, W., Ali, M. A. H. (2024). Prediction of compressive strength of recycled concrete using gradient boosting models. *Ain Shams Engineering Journal*, 15(9): 102975.

[25] Alessandro Pansera, W., Alessi Reichert, T., Savaris, G., Eduardo Tino Balestra, C. (2022). Nonlinear regression using Gaussian-Lorentzian functions to empirical modeling of convective-diffusive chloride transport in concrete. *Construction and Building Materials*, 341: 127770.

[26] Mesfin, W. M., Kim, H. K. (2024). Parametric study on global estimation models for compressive strength adopting various machine learning algorithms in concrete. *Engineering Applications of Artificial Intelligence*, 136: 108888.

[27] Le, H. V., Kim, M. K., Kim, S. U., Chung, S. Y., Kim, D. J. (2021). Enhancing self-stress sensing ability of smart ultra-high performance concretes under compression by using nano functional fillers. *Journal of Building Engineering*, 44: 102717.